An Analytical Method to Study the Effects of a Substrate in Surface-Enhanced Raman Scattering

Shao Ying Huang[1,2], Bae-Ian Wu[1],* Baile Zhang[1], Yee Hui Lee[2], Vladimir Liberman[3], and Mordechai Rothschild[3†]

[1]*Research Laboratory of Electronics, Massachusetts Institute of Technology, Cambridge, MA 02139-4307, USA*

[2]*School of Electrical and Electronic Engineering, Nanyang Technological University, Singapore 639798 and*

[3]*Lincoln Laboratory, Massachusetts Institute of Technology, Lexington, MA 02420, USA*

(Dated: October 20, 2009)

Abstract

In studies of surface-enhanced Raman Scattering (SERS), individual metal nanoparticle and particle assemblies introduce enhancement of electromagnetic fields. However, the contributions to enhancement due to the substrate supporting the particles are yet to be studied analytically. In this communication, we present an analytical method to investigate the effect of a substrate with realistic layers in SERS. The proposed method quantifies the effect of a substrate on the electric field on the nanoparticles surface in SERS experiments. By applying the proposed method, optimal constructions of a substrate can be obtained to maximize the surface electric field while a poorly constructed one can be avoided. The maximization can lead to a high Raman enhancement factor. The method is verified using numerical simulations.

*Electronic address: biwu@mit.edu

†The Lincoln portion of this work was sponsored by the Defense Advanced Research Projects Agency under Air Force Contract FA8721-05-C-0002. Opinions, interpretations, conclusions, and recommendations are those of the author, and do not necessarily represent the view of the United States Government.

I. INTRODUCTION

Surface-enhanced Raman scattering (SERS) has recently been the subject of renewed interest, more than 30 years after the original observation of this effect. This strong interest, both in the experimental and simulation areas, is attributable to progress toward the practical realization of SERS, enabled by new nanofabrication techniques [1][2]. Besides the technology "push", there has been of course growing interest on the application "pull" side for chemical sensing and biomolecule analysis.

In 1997, by using SERS, single molecules and single nanoparticles were successfully detected [3][4]. The measured Raman enhancement factor has since been reported to be as high as 10^{14}–10^{15}, although controllable and repeatable experiments have been difficult to achieve at these high enhancement levels. The Raman enhancement is attributed to two main mechanisms, namely electromagnetic field enhancement and chemical enhancement, with the electromagnetic mechanism providing the dominant contribution to the SERS effect. This mechanism is prominent when plasmon resonance excitation in the nanoparticle generates an enhanced electric field (E-field) on the particle surface, which in turn leads to enhanced Raman excitation of surface adsorbed molecules [5]. A large variety of structures are observed or predicted to have a large Raman enhancement factor. For example, nanoparticles suspended in solutions [4] or immobilized on substrate such as Si or glass [3][6], or nanoslits etched in planar metal films [7]. It is well established that the electric field is locally affected by the geometry of the nanoparticles, but it must be noted that it is also globally affected by the particles in the neighborhood or by the substrate supporting the particles.

Due to the dominant effect of the electromagnetic enhancement mechanism in SERS, electromagnetic theories analyzing the E-fields around the nanoparticles are useful in providing basic guidance to obtain a high Raman enhancement factor. For an isolated spherical nanoparticle, Mie theory provides an analytical solution. Numerically, finite-difference time-domain (FDTD) methods and other computational electrodynamic methods such as discrete dipole approximation (DDA) [8] are available to determine the local E-fields by solving Maxwell's equations. Based on numerical calculations, it is found that dimers, which consist of two nanoparticles in close proximity to each other, show a much higher Raman enhancement factor as compared to monomers where only one single nanoparticle

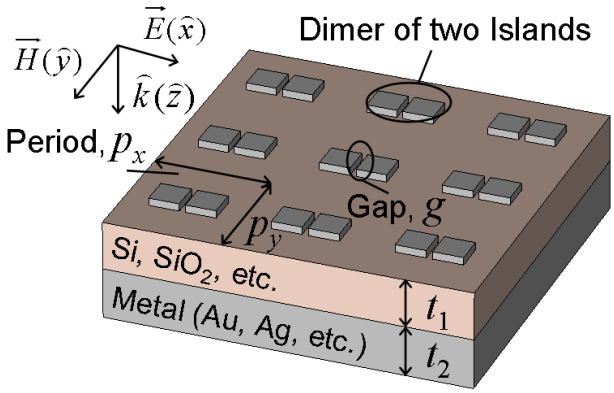

(a) 3D view

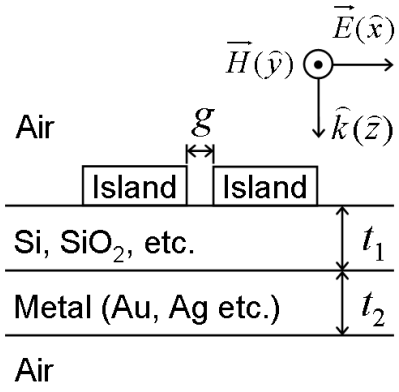

(b) 2D side view of the unit cell of a dimer

FIG. 1: Periodic dimers on a layered substrate.

is considered [9]. It has also been reported that an extra factor of 10^2 can be added when taking into account long-range coupling effects introduced by an aggregate [10] or an array of nanoparticles [11].

In most of the recent SERS experiments, metal particles are immobilized on a dielectric substrate for the detection of scattered SERS signals [3][6]. However, while the effect of the substrate supporting the nanoparticles can be approximated numerically using DDA [8], many of the numerical results calculate only localized fields near the surface of isolated particles, where the particles are assumed to be surrounded by homogeneous dielectric medium, without considering the effect of the substrate [9][12]. An exception is [13], where the effect of the substrate is studied experimentally and numerically. This study was conducted by changing substrates of different refractive indices, and the effect of the refractive index of

the substrate is reported in detail.

In this report, we present an analytical method to quantify the effect of a substrate on the surface E-field of nanoparticles in SERS. This approach provides fundamental guidance to the construction of a full SERS device, including nanoparticles and the supporting substrate. It can be used to maximize the E-field available on the surface of the nanoparticles and to avoid a cancelation of the fields. The maximization can contribute to a considerable increase in the overall Raman enhancement factor.

II. ANALYTICAL METHOD

An ideal SERS substrate may consist of a periodic array of nanostructures, each consisting of a dimer of metal nano-islands, on a layered substrate. Fig. 1 (a) and (b) show the three-dimensional (3D) view of such an array on top of a layered substrate and the 2D side view of the unit cell of a dimer, respectively. As can be seen in Fig. 1 (a), a dimer has two islands with a gap of distance g between them. They are repeated with a periodicity in the $\hat{x}$- and $\hat{y}$-directions, p_x and p_y, respectively. They are located on a substrate comprising a dielectric layer of thickness t_1 and a metal layer of thickness t_2. The dielectric material can be Si or SiO_2 [3][6] whereas the metal at the bottom can be gold, silver, aluminum etc. Fig. 1 (b) shows the side view of the unit cell of a dimer when viewed along the $\hat{y}$-direction (either positive or negative). In what follows, however, we will analyze only arrays of monomers, since our goal is to highlight the effect of the substrate and the fractional composition of the array layer. Further optimization of the array nanostructures, for instance by designing dimers in the unit cell, is the subject of separate studies.

A. E-Fields on the Surface of a Substrate

The effect of a substrate on the E-field available on the surface of metal nanoparticles is global as compared to the effect due to the metal nanoparticle on the localized E-fields near the particles. Therefore, in the first stage of the analysis, we study the effect of a substrate on the E-fields on the surface of the substrate, while the islands are temporarily ignored. Fig. 2 shows this geometry. The substrate consists of a Si- and a Au-layer with a boundary at $z = d_1$ between them. They are both assumed to be homogeneous and infinite in the

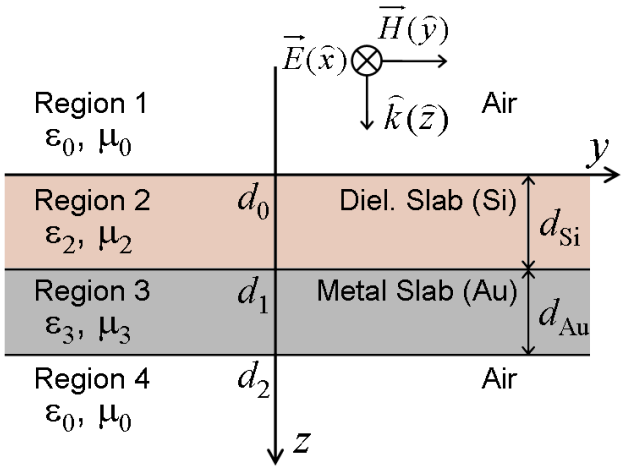

FIG. 2: Schematic of the layered substrate.

$\hat{x}$-direction, thus fringing fields can be neglected and $\partial/\partial x = 0$. The thickness of the Si-layer on the top is d_{Si} ($d_{\mathrm{Si}} = d_1 - d_0$) and that of the Au-layer at the bottom is d_{Au} ($d_{\mathrm{Au}} = d_2 - d_1$). The substrate has a surface at $z = d_0$ and a bottom at $z = d_2$. It splits the space into four regions as numbered in Fig. 2. Region 1 and Region 4 are filled with air. The relative permittivity and permeability of the material in the n^{th} region are denoted as ϵ_n and μ_n, respectively, where $n = 1$, 2, 3, and 4. The permittivity and permeability of air are ϵ_0 and μ_0, respectively.

When a TEM plane wave is normally incident onto the stratified substrate as shown in Fig. 2, the total field in region n can be expressed as [14]

$$\overline{E}_n = \hat{x}(A_n e^{ik_n z} + B_n e^{-ik_n z}) \tag{1}$$

$$\overline{H}_n = \frac{1}{w\mu_n\mu_0}\overline{k}_n \times \overline{E}_n \tag{2}$$

where $\overline{k}_n$ is the wave vector and $\overline{E}_n$ is the E-field strength. A_n and B_n are the E-field amplitudes of the downward and upward waves, respectively. $\overline{H}_n$ is the magnetic field strength. Subscript n indicates the n^{th} region.

For a propagating plane wave, the E-field amplitude of the upward wave in Region 4 is $B_4 = 0$, and A_1 in Region 1 is assumed to be 1 for the purpose of normalization. In each region, A_n and B_n are related by boundary conditions. At $z = d_n$, E_x and H_y are continuous. By matching boundary conditions, a recurrent expression for B_n/A_n can be

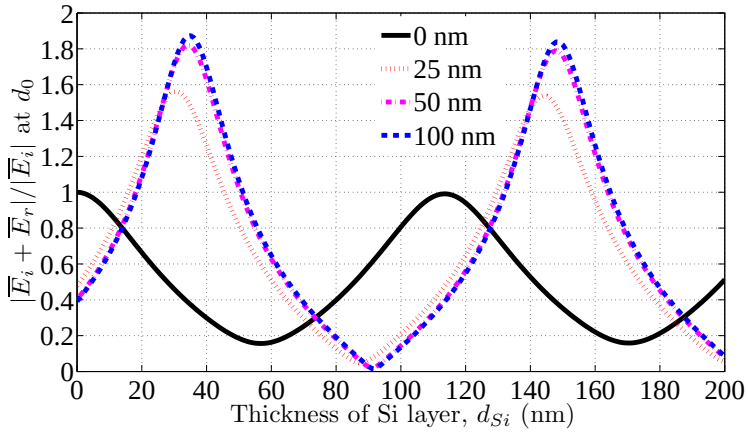

FIG. 3: The normalized magnitude of the E-fields on the surface of the substrate ($z = d_0$) when the thickness of the Si-layer is varied and $d_{\mathrm{Au}} = 0$ nm, 25 nm, 50 nm, and 100 nm.

obtained as below [14],

$$\frac{B_n}{A_n} = \frac{R_{n(n+1)} e^{i2k_{n+1}d_n} + (B_{n+1}/A_{n+1})}{e^{i2k_{n+1}d_n} + R_{n(n+1)}(B_{n+1}/A_{n+1})} e^{i2k_n d_n} \tag{3}$$

where

$$R_{n(n+1)} = \frac{1 - p_{n(n+1)}}{1 + p_{n(n+1)}} \tag{4}$$

$$p_{n(n+1)} = \frac{\mu_n k_{n+1}}{\mu_{n+1} k_n} \tag{5}$$

and B_n/A_n is expressed in terms of B_{n+1}/A_{n+1}. Therefore, with an incident wave propagating towards the slab, the reflected E-field can be obtained at any point along the z axis when the parameters of the material and the thickness of each layer are known.

Next, the effect of d_{Si} and d_{Au} on the E-fields at $z = d_0$ is studied. A TEM plane wave at 785 nm incident normally towards the stratified substrate in the $\hat{z}$-direction is considered. The permeabilities, μ_2 and μ_3 both equal to 1. The loss tangent of Si is 0.004 and its relative permittivity, ϵ_2, is 11.92 + 0.04i at 785 nm. The relative permittivity of Au at 785 nm is $-24.70 + 1.76$i [15]. Based on (3)–(5), the magnitude of the sum of E-fields at $z = d_0$, including the incident and the reflected E-fields, is calculated when the thickness of the Si-layer is varied and $d_{\mathrm{Au}} = 0$ nm, 25 nm, 50 nm, and 100 nm. As $A_1 = 1$, the sum of the E-fields is normalized and can be expressed as $|\overline{E}_i + \overline{E}_r|/|\overline{E}_i|$, where $\overline{E}_i$ and $\overline{E}_r$ are the incident and the reflected E-fields, respectively. The calculated results are plotted in Fig. 3.

In Fig. 3, the solid line depicts the magnitude of the E-fields on the surface of the substrate when there is no Au-layer at the bottom ($d_{\mathrm{Au}} = 0$ nm). When $d_{\mathrm{Si}} = 0$ nm and there is no

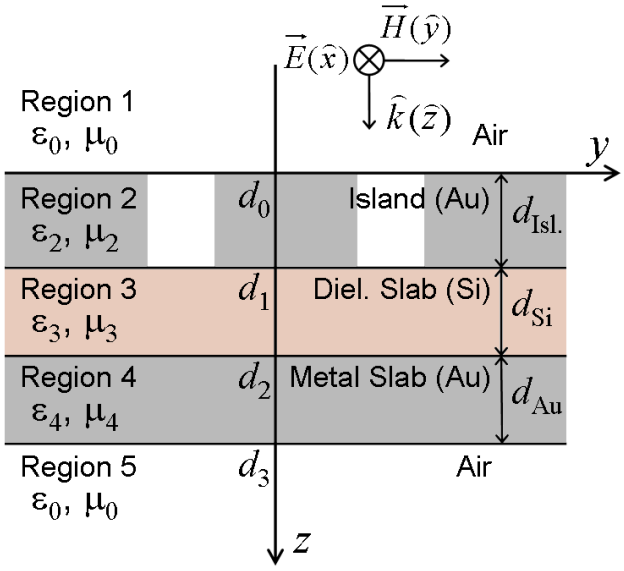

FIG. 4: Schematic of the layered substrate with an island-layer.

substrate, the magnitude of the E-field is 1.00. This magnitude varies between 0.16 to 1.00 as the thickness of the Si-layer changes from 0 nm to 200 nm. It has the first peak value of 1.00 at $d_{\mathrm{Si}} = 0$ nm, the first minimum value of 0.16 at $d_{\mathrm{Si}} = 57$ nm, and the second peak value of 0.99 at $d_{\mathrm{Si}} = 114$ nm. The peak values decreases as the thickness of the Si-layer increases, which is due to absorptive losses in Si. When a Au-layer is incorporated into the substrate, the maximum magnitude of the E-field available on the surface of the substrate increases significantly, as shown by the other lines in Fig. 3. We note that, in all cases with a finite Au-layer, the magnitude of the E-field varies between 0 and 2 as d_{Si} varies. When the thickness of the Au-layer is 100 nm, as shown by the dashed line in Fig. 3, the magnitude of the E-field varies from 0.01 to 1.87 when d_{Si} varies. It has peak values of 1.87 and 1.84 when d_{Si} is 35 nm and 148 nm, respectively. As in the case when there is no Au-layer in the substrate, the peak value decreases as d_{Si} increases, owing to the losses in Si. When the thickness of the Au-layer at the bottom decreases, the maximum magnitude of the E-field at $z = d_0$ decreases. When $d_{\mathrm{Au}} = 50$ nm, the magnitude has a maximum and a minimum value of 1.82 and 0.02 at $d_{\mathrm{Si}} = 34$ nm and 91 nm, respectively. When $d_{\mathrm{Au}} = 25$ nm, the maximum magnitude is found to be 1.56 at $d_{\mathrm{Si}} = 31$ nm while the minimum value is 0.05 at $d_{\mathrm{Si}} = 87$ nm. The thickness of the Si-layer where the maximum E-field is found decreases as d_{Au} decreases.

The results above clearly indicate that the thicknesses of both the Si-layer and the Au-layer in the substrate play an important role in determining the magnitude of the E-field on

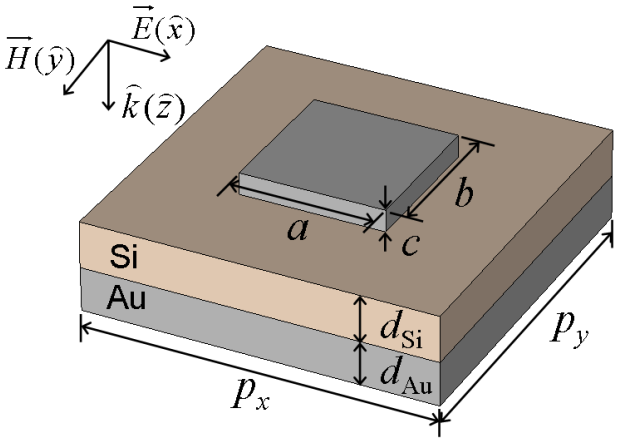

FIG. 5: 3D view of the unit cell of a monomer.

the surface of the substrate. The magnitude of the E-field depends on the properties of the materials, the thickness of each layer, and the frequency of the wave. Without a Au-layer at the bottom, there is no gain of total incident E-field on the surface of the substrate. Moreover, the thickness of the Si-layer should be set appropriately in order to avoid a large cancelation by the reflected wave (to avoid the points where $|\overline{E}_i + \overline{E}_r|/|\overline{E}_i|$ is minimum). By using a Au-layer, the available E-field on the surface of the substrate can reach a factor of 1.8 or more of the incident E-field (capped by a factor of 2). Using this method, an optimal thickness of each layer can be obtained analytically so as to maximize the E-field on the surface of the substrate.

B. E-Fields on the Surface of Nanoparticles

In the next stage of our analysis, the E-field on the surface of the nanoparticles is studied by adding islands onto the substrate. The islands form an additional layer that we call island-layer. Fig. 4 shows the schematic of an island-layer on top of the substrate that was studied previously. The island-layer extends from $z = d_0$ to $z = d_1$. Its thickness is $d_{\mathrm{Isl.}}$ ($d_{\mathrm{Isl.}} = d_1 - d_0$). Following the same analytical method introduced in the previous section, with the known permittivity, permeability, and thickness of each layer, the magnitude of the E-field on the surface of the nanoparticles ($z = d_0$) can be obtained using (3)–(5) above.

The relative permittivity of the island-layer, ϵ_2, is an effective permittivity which depends on the percentage of islands in a unit cell. The Maxwell Garnett equation shown below is

used to estimate the effective permittivity, ϵ_2 [16].

$$\epsilon_{eff} = \epsilon_b[\frac{1 + 2f(\epsilon_i - \epsilon_b)/(\epsilon_i + 2\epsilon_b)}{1 - f(\epsilon_i - \epsilon_b)/(\epsilon_i + 2\epsilon_b)}] \tag{6}$$

where f is the fraction of the metallic inclusion (the islands) in the island-layer, ϵ_i and ϵ_b are the permittivity of the inclusion and of the background material, respectively. The fraction f is determined by the volume of the nanoparticle and its periodicities, p_x and p_y [see Fig. 1].

As an example, periodic monomers with a square island in each unit cell are studied. Fig. 5 shows the 3D view of such a monomer where a, b, and c are the length of the monomer in the $\hat{x}$-, $\hat{y}$-, and $\hat{z}$-directions, respectively ($c = d_{\text{Isl.}}$). The dimension of the monomer in the $\hat{x}$- and $\hat{y}$-directions, a and b, respectively, are both set to be 164.4 nm and the periodicities, p_x and p_y, are both set to be 400 nm. The fraction f is determined to be 16.89% with air as the background material. $\epsilon_2 = \epsilon_{eff}$ is calculated to be $1.717 + 0.004\text{i}$. Based on (3)–(5), the magnitude of the E-field on the nanoparticle surface ($z = d_0$) is calculated when $f = 16.89\%$ and compared to the case without islands, i.e., $f = 0\%$. The thickness of the island-layer is set to be 25 nm and that of the Au-layer at the bottom is set to be 50 nm. Fig. 6 (a) shows the calculated magnitudes of the E-fields versus the thickness of the Si-layer. The case when $f = 16.89\%$ and there is no Au-layer at the bottom of the substrate ($d_{\text{Au}} = 0$ nm) is also included.

As shown in Fig. 6 (a), when $f = 16.89\%$ and no Au-layer is at the bottom, the E-field is 0.98 when $d_{\text{Si}} = 0$ nm. This means that the E-field available on the surface of the islands (nanoparticles) has a magnitude of less than one when no substrate is supporting the islands. It is not the maximum value of E-field in this case. As shown by the same curve in Fig. 6 (a), when d_{Si} increases and the islands are located on a Si slab, the magnitude of the E-field on the surface of the islands varies. It has the first minimum value of 0.21 at $d_{\text{Si}} = 36$ nm and a maximum value of 1.05 at $d_{\text{Si}} = 106$ nm. When there is a 50 nm-Au-layer at the bottom and $f = 16.89\%$, the maximum magnitude increases significantly, which is shown by the dashed curve in Fig. 6 (a). In this case, the magnitude of the E-field varies from 1.83 to 0.03 when $d_{\text{Si}} = 30$ nm and 68 nm, respectively. The magnitude changes considerably for different thicknesses of the Si-layer. As revealed by these results, nanoparticles with a reflecting Au-layer have an additional enhancement factor of the E-field of 1.74 (1.83/1.05) over the case without a Au-layer. Comparing within the case when $d_{\text{Au}} = 50$ nm, an optimal substrate is possible to be obtained providing an additional enhancement factor of the E-field of more

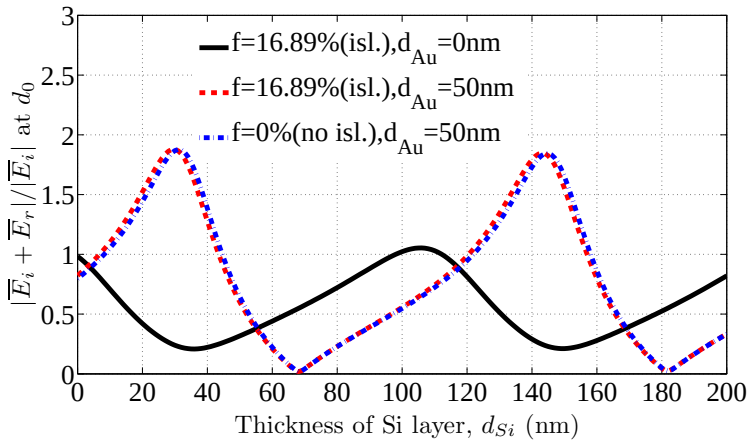

(a) Islands (isl.) on Si-layer

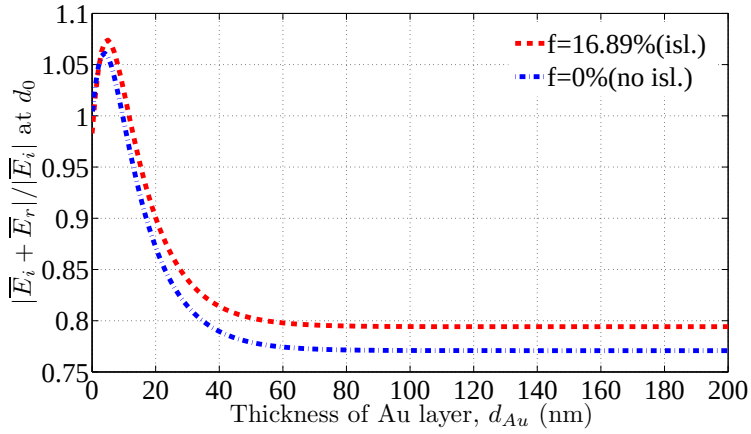

(b) Islands on Au film

FIG. 6: The normalized magnitude of the electric field at the first boundary ($z = d_0$) of the layered substrate in Fig. 4.

than 50 (1.83/0.03) over a poorly constructed substrate. This is equivalent to a differential factor of $(|\overline{E}|/|\overline{E}_i|)^4 > 10^7$ $((1.83/0.03)^4)$ where $\overline{E}$ is the total E-field on the surface of the nanoparticles.

At $f = 0\%$, the magnitude of the E-field has a maximum value of 1.83 at $d_{\mathrm{Si}} = 32$ nm, which is close to that at $f = 16.89\%$. Thus, in these two cases where Si is in the middle of the island-layer and the Au-layer, the maximum E-field and d_{Si} corresponding to the maximum do not vary much as the percentage of the islands in the island-layer changes ($f \leq 16.89\%$). The difference in d_{Si} could be large if Si is replaced by other dielectric materials such as

TABLE I: E-fields on the Surface of Nanoparticles (on Si-Layer)

d_{Si} (nm)	Max.$\lvert\overline{E}\rvert/\lvert\overline{E}_i\rvert$ (CST)	$\lvert\overline{E}_i+\overline{E}_r\rvert/\lvert\overline{E}_i\rvert$ at $z=d_0$
15	10.25	1.25
30	18.90	1.83
50	5.18	0.61
68	3.11	0.03

TABLE II: E-fields on the Surface of Nanoparticles (on Si-Layer, Optimized)

$a=b$ (nm)	d_{Si} (nm)	Max.$\lvert\overline{E}\rvert/\lvert\overline{E}_i\rvert$ (CST)
222.5	30	20.66
40	68	0.54

SiO_2. Here we have analyzed Si specifically, because of its good thermal conductivity.

In the case where metal nanoparticles are deposited directly onto a metal film, this model also provides estimations of the global effect of the substrate. In this case, d_{Si} in Fig. 4 is set to be zero. Fig. 6 (b) shows the calculated magnitude of the E-field at $z=d_0$ when islands (164.4 nm $\times$164.4 nm $\times$25 nm) are located on top of a Au film at a periodicity of 400 nm in both the $\hat{x}$- and $\hat{y}$-directions. The horizontal axis in Fig. 6 (b) is the thickness of the Au film. Both cases when $f=16.89\%$ and $f=0\%$ are included. At $f=16.89\%$, the magnitude of the E-field has a peak value of 1.08 at $d_{\mathrm{Au}}=5$ nm and it is largely unchanged at $d_{\mathrm{Au}}>60$ nm. At $f=0\%$, the peak value of the magnitude is 1.06 when the thickness of the Au film is 4 nm. It is also unchanged at $d_{\mathrm{Au}}>60$ nm. For Au nanoparticles on Au film, the optimal thickness of the metal film does not vary significantly as the percentage of the nanoparticles in the island-layer changes ($f\leq 16.89\%$).

III. COMPUTATIONAL VERIFICATIONS

The analytical results obtained in the previous section are verified using a numerical simulation tool, CST Microwave Studio [17]. Fig. 5 shows the 3D view of the unit cell of a

TABLE III: E-fields on the Surface of Nanoparticles (on Au-Layer)

d_{Au} (nm)	Max.$\lvert\overline{E}\rvert/\lvert\overline{E}_i\rvert$ (CST)	$\lvert\overline{E}_i+\overline{E}_r\rvert/\lvert\overline{E}_i\rvert$ at $z=d_0$
5	8.58	1.07
20	5.17	0.90
60	4.79	0.80
80	2.38	0.80
100	3.67	0.80

monomer under simulation. The dimensions of the monomer in the $\hat{x}$- and $\hat{y}$-directions, a and b are both fixed at 164.4 nm and the thickness of the island, c is 25 nm ($c = d_{\mathrm{Isl.}}$). The period is 400 nm in both the $\hat{x}$- and $\hat{y}$-directions. The thickness of the Au-layer at the bottom, d_{Au} is 50 nm, and d_{Si} is set to be 15 nm, 30 nm, 50 nm, and 68 nm. The simulated maximum magnitude of the E-fields on the surface of the monomer are extracted, normalized to that of the incident E-field, and tabulated in Table I. The calculated magnitude of the E-fields at the corresponding d_{Si} are extracted from Fig. 6 (a) and tabulated in Table I. In the simulation results, the dimension of the island in the $\hat{x}$-, $\hat{y}$-, and $\hat{z}$-directions and the periodicity in the $\hat{x}$- and $\hat{y}$-directions affect the E-field on the surface of the islands. Therefore, the simulated $|\overline{E}|/|\overline{E}_i|$ includes both the local effect in each direction and the global effects in both the $\hat{x}$- and $\hat{y}$-directions. This is a more accurate depiction of the E-field behavior than the analytical calculations in Section II above, which address only global effects. Nevertheless, the trends are quite similar, as shown in Table I. When d_{Si} is changed, the simulation results still show an increase and then a decrease, with CST-calculated absolute values being $\sim 8-10\times$ higher than those obtained by the analytical method.

The dimensions of the islands on top of a 30 nm- and 68 nm-Si-layer can be further optimized to obtain local resonances at 785 nm in each case, by changing the dimensions of the island. In these simulations, there is a 50 nm Au-layer at the bottom. Table II shows the simulated normalized E-fields in both cases. As can be seen in Table II, the substrate affects the local resonance in the island. A 222.5 nm $\times$222.5 nm $\times$25 nm island on 30 nm-Si-layer has a resonance at 785 nm and it shows a maximum normalized magnitude of the

E-field of 20.66. On the other hand, the monomer on 68 nm-Si-layer has a resonance at the same wavelength when the island has a dimensions of 40 nm, 40 nm, and 25 nm in length, width, and height, respectively. It shows $|\overline{E}|/|\overline{E}_i| = 0.54$. The results reveal that, even at the local resonance of the monomer that has a 68 nm-Si-layer, the monomer with an optimal 30 nm-Si-layer can provide a factor of 38.26 for the enhancement of the E-field over that of the 68 nm-Si-layer. The factor of 38.26 for the enhancement of the E-field corresponds to a SERS enhancement factor of $(|\overline{E}|/|\overline{E}_i|)^4 > 10^6$. This comparison indicates that the effect of a substrate in SERS can even overshadow the local effects and can become very significant. Therefore, this effect cannot be neglected and should be carefully addressed in any design of SERS devices.

Au nanoparticles on a Au film were also simulated with fixed dimensions of the monomer (164.4 nm × 164.4 nm × 25 nm), while the thickness of the Au film was varied. The periodicities, p_x and p_y were both fixed at 400 nm. Table III shows the simulated normalized magnitudes of the E-fields on the surface of the nanoparticles when the periodic monomers are located directly on a Au film. It also tabulates the extracted calculated magnitudes of the E-fields at the corresponding thicknesses of the Au film using the proposed analytical method. Since the dimension of the island and the periodicity are fixed in the simulations, the local and the global effects in the $\hat{x}$- and $\hat{y}$-directions still remain. While the absolute values shown in Table III differ, the trend of the computationally obtained data is in good qualitative agreement with that of the results based on the proposed analytical method of Section II. The fluctuations in the computationally simulated results when $d_{\mathrm{Au}} \geq 60$ nm may be caused by the local resonances in the islands, and these are of course not accounted for in the analytical model.

IV. CONCLUSION

We have proposed an analytical method to study the global effect of a substrate on the surface electric field of nanoparticles in SERS. The effect of the substrate is quantified in terms of the parameters of material and thickness of each layer. A Au-layer at the bottom of the substrate provides an additional factor of 1.7 of the magnitude of the E-field over that when there is no Au-layer incorporated. By applying the analytical method, an optimal construction of the substrate can be obtained while a poor one can be avoided. An

optimized substrate results in an E-field that is a factor of more than 50 higher than that of a poorly constructed one. A substrate consisting of a Si-layer and a Au-layer, as well as the case where nanoparticles are directly located on a Au film, are both analyzed. It is shown that the global effect of the substrate can become significant and even overshadow the strong local electromagnetic effects in SERS. An optimized substrate can contribute to a significant increase in the Raman enhancement factor.

Acknowledgments

The Research Laboratory of Electronics portion of this work was supported by MIT Lincoln Laboratory under Contract No. FA8721-05-C-0002. The Lincoln Laboratory portion of this work was sponsored by the Defense Advanced Research Projects Agency under Air Force Contract FA8721-05-C-0002. Opinions, interpretations, conclusions, and recommendations are those of the author, and do not necessarily represent the view of the United States Government.

---

[1] R. Jin, Y. Cao, C. A. Mirkin, K. L. Kelly, G. C. Schatz, and J. G. Zhang, Science **294**, 1901 (2001).

[2] C. L. Haynes and R. V. Duyne, J. Phys. Chem. B **105**, 5599 (2001).

[3] S. Nie and S. R. Emory, Science **275**, 1102 (1997).

[4] K. Kneipp, Y. Wang, H. Kneipp, L. T. Perelman, I. Itzkan, R. R. Dasari, and M. S. Feld, Physical review letters **78**, 1667 (1997).

[5] K. Kneipp, M. Moskovits, and H. Kneipp, *Surface-enhanced Raman scattering, physics and applications* (Springer, 2006).

[6] M. Futamata, Y. Maruyama, and M. Ishikawa, Vibrational spectroscopy **35**, 121 (2004).

[7] J. T. Bahns, A. Imre, V. K. Vlasko, J. Pearson, J. M. Hiller, L. H. Chen, and U. Welp, Applied physics letters **91**, 081104 (2007).

[8] W. Yang, G. C. Schatz, and R. P. V. Duyne, The Journal of Chemical Physics **103**, 869 (1995).

[9] E. Hao and G. C. Schatz, The Journal of Chemical Physics **120**, 357 (2004).

[10] W. Kim, V. P. Safonov, V. M. Shalaev, and R. L. Armstrong, Physical review letters **82**, 4811 (1999).

[11] S. Zou and G. C. Schatz, Chemical Physics Letters **403**, 62 (2005).

[12] K. Li, L. Clime, L. Tay, B. Cai, M. Geissler, and T. Veres, Analytical Chemistry **80**, 4945 (2008).

[13] M. D. Malinsky, K. L. Kelly, G. C. Schatz, and R. P. V. Duyne, The Journal of Physiccal Chemistry **105**, 2343 (2001).

[14] J. A. Kong, *Electromagnetic Wave Theory* (EMW Publishing, 2008).

[15] E. D. Palik, *Handbook of optical constants of solids* (San Diego : Academic Press, 1998).

[16] A. H. Sihvola and J. A. Kong, IEEE Transactions on geoscience and remote sensing **26**, 420 (1988).

[17] *CST MICROWAVE STUDIO^{TM} 5.0* (CST of Ametica, Inc., www.cst.com, 2005).